A.

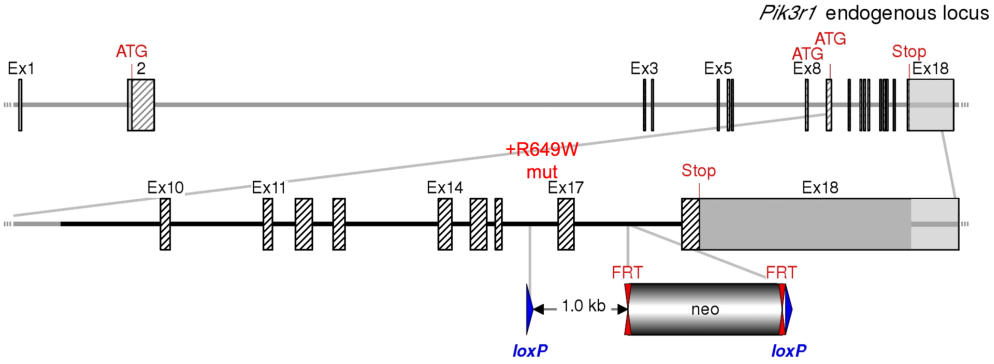

B.

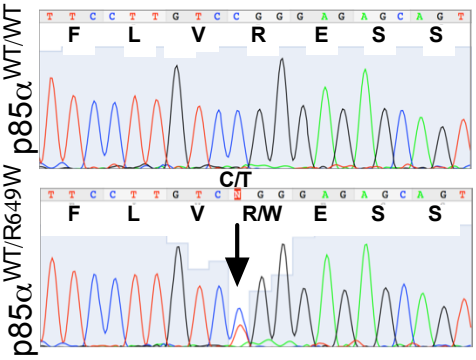

Supplemental Figure 1. Targeting strategy and confirmation of *Pik3R1* mutation. (**A**) Diagram of targeting strategy for generation of *Pik3R1* R649W mutation. Diagram is not depicted to scale. Hatched rectangles represent Pik3r1 coding sequences, grey rectangles indicate non-coding exon portions, solid lines represent chromosome sequences. The neomycin positive selection cassette is indicated. loxP sites are represented by blue triangles and FRT sites by red double triangles. The three initiation codons (ATG) for the full-length and alternatively spliced products of the *Pik3R1* gene as well as the stop (Stop) codon are indicated. Presented with permission from Genoway. (**B**) DNA sequence chromatograms of genomic DNA isolated from p85a$^{WT/WT}$ and p85a$^{WT/R649W}$ mice confirming the mutation.

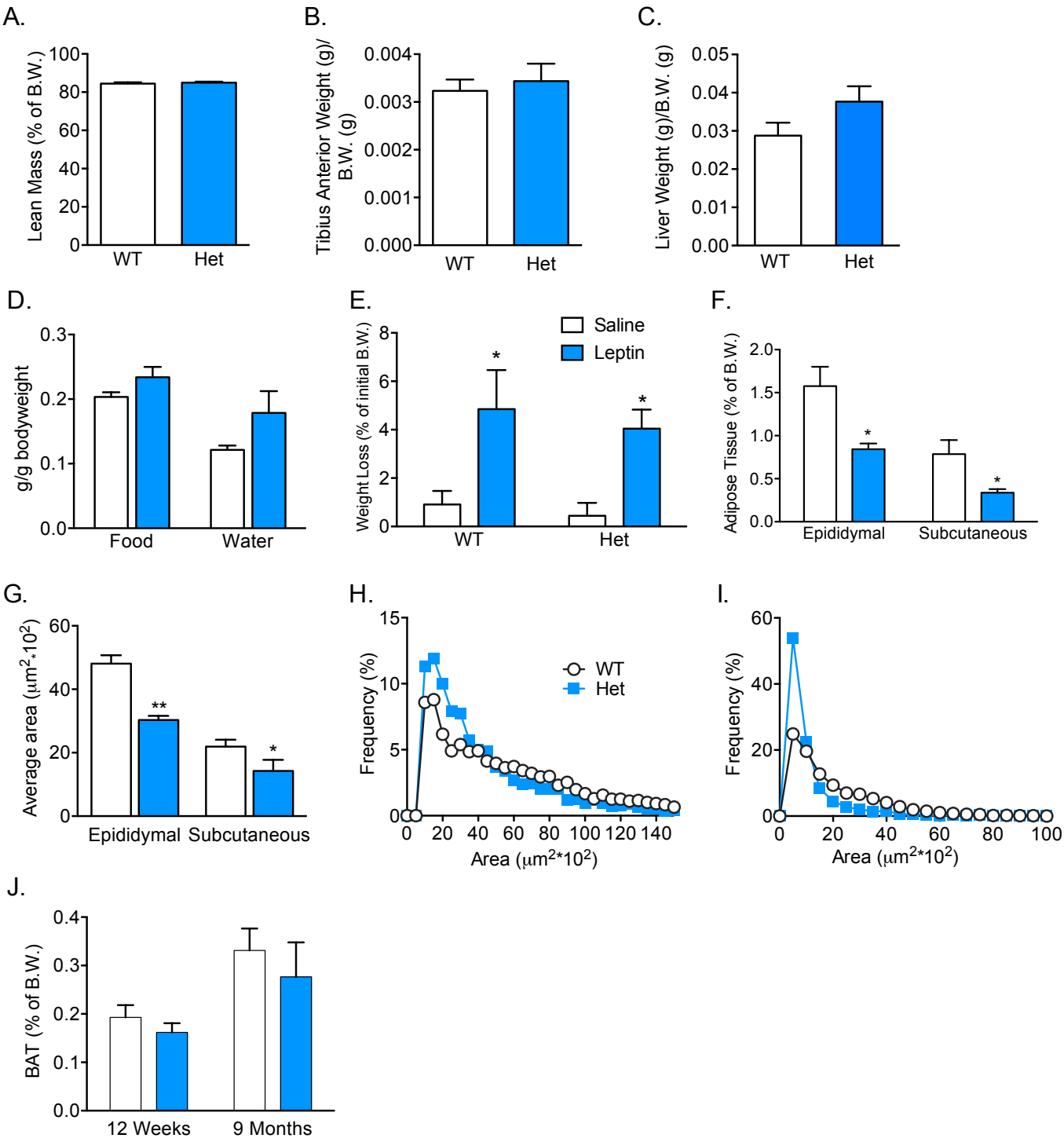

Supplemental Figure 2. p85$^{WT/R649W}$ mice show a selective reduction in subcutaneous adipose tissue mass. (**A**) Lean mass assessed by DEXA analysis and (**B**) tibialis anterior weight (N=9-11) and (**C**) liver weight of p85$^{WT/WT}$ and p85$^{WT/R649W}$ animals (N=3) at 12 weeks of age. (**D**) Food and water intake of mice at 12 weeks of age. (**E**) Reduction in body weight in mice treated with saline or leptin (4 mg/kg) for 72 hours. Results are shown as mean ± SEM of 9-12 mice per group. (**F**) Adipose tissue from 9 month old male animals expressed as a % of body weight. (N=5) (**G**) Average adipocyte area in epididymal and subcutaneous adipose tissues in male p85$^{WT/WT}$ and p85$^{WT/R649W}$ mice at 9 months of age. (N=7-9) Average adipocyte area distribution from (**H**) epididymal and (**I**) subcutaneous adipose tissue. (N=4) (**J**) Brown adipose tissue weights expressed as % of body weight at 12 week and 9 months of age in male study group mice. (N=5) Results are shown as mean ± SEM, * $p<0.05$, ** $p<0.01$)

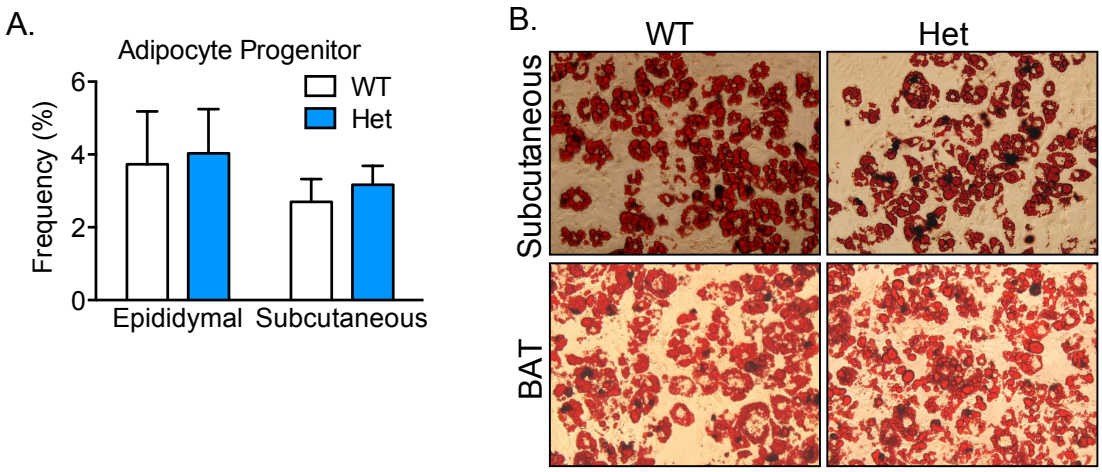

Supplemental Figure 3. Adipocyte progenitor number and pre-adipocyte differentiation potential are not altered in p85$^{WT/R649W}$ mice. (A) Adipocyte progenitor cells were quantified from the stream vascular fraction obtained from epididymal and subcutaneous adipose tissue by flow cytometry (N=4). (**B**) Oil Red O staining of differentiated stromal vascular cells obtained from subcutaneous or brown adipose tissue of study group mice (40X)(N=3).

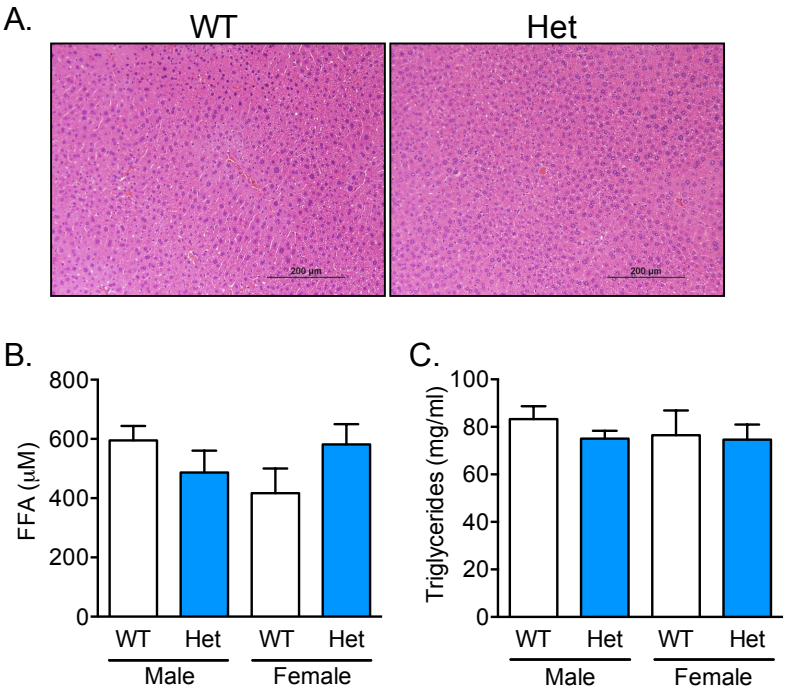

Supplemental Figure 4. p85$^{WT/R649W}$ mice do not exhibit liver steatosis. (**A**) Hematoxylin and eosin-stained liver tissue sections from female p85$^{WT/WT}$ and p85$^{WT/R649W}$ study group animals at 1 year of age (20X). Circulating (**B**) free fatty acid and (**C**) triglycerides levels in random-fed 1 year old mice (N=5-9). Results are shown as mean ± SEM.

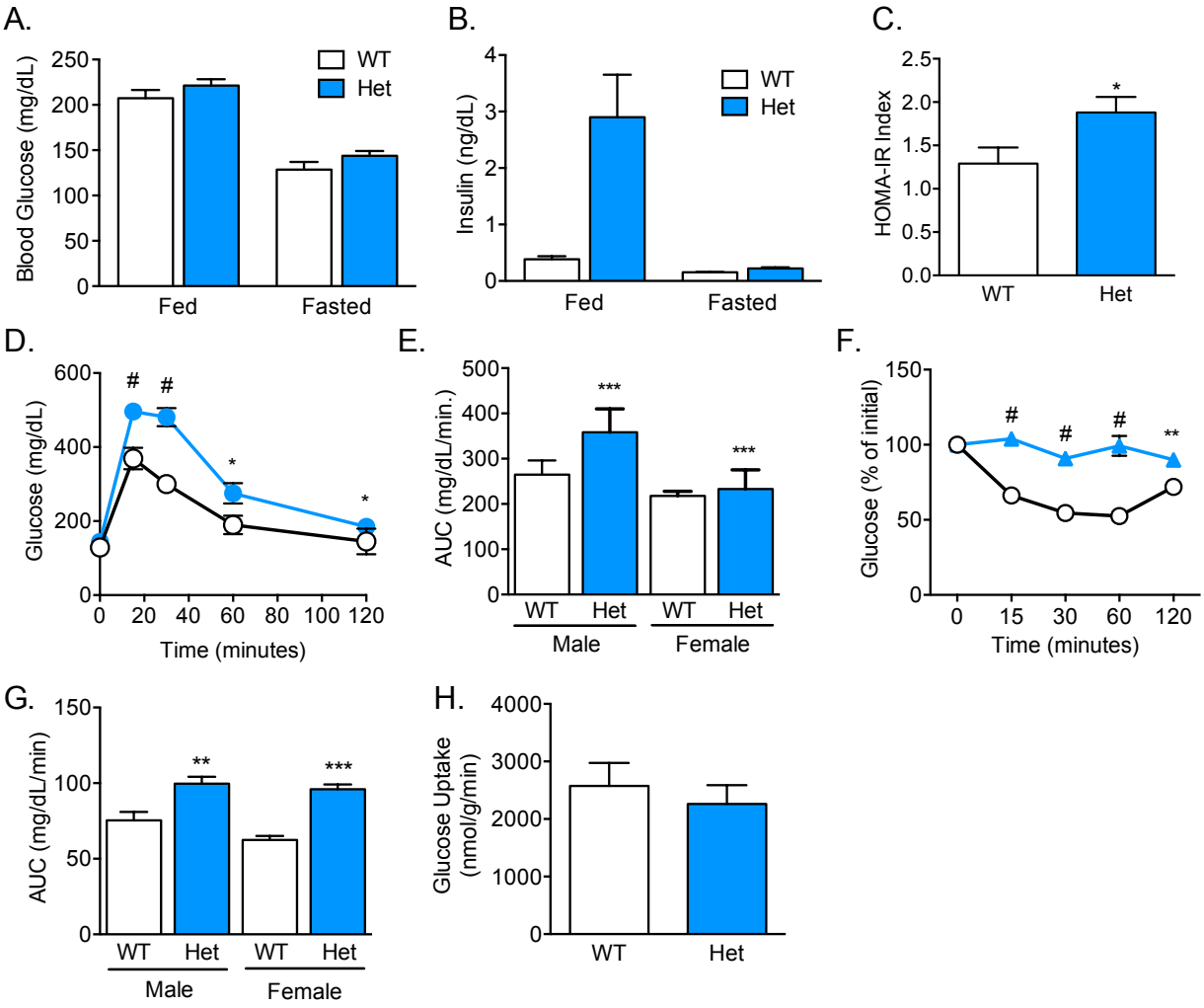

Supplemental Figure 5. Female p85$^{WT/R649W}$ are hyperinsulinemic and insulin resistant. (A) Blood glucose and **(B)** insulin levels in the fed and fasted states in female study group animals at 8 weeks of age. **(C)** HOMA-IR index calculated using fasting glucose and insulin levels. Results of glucose **(D,E)** and insulin tolerance **(F,G)** tests**.** Results are expressed as mean ± SEM (N=9-12 per group). (*, $p<0.05$; **, $p<0.01$; ***, $p<0.001$; #, $p< 0.0005$).

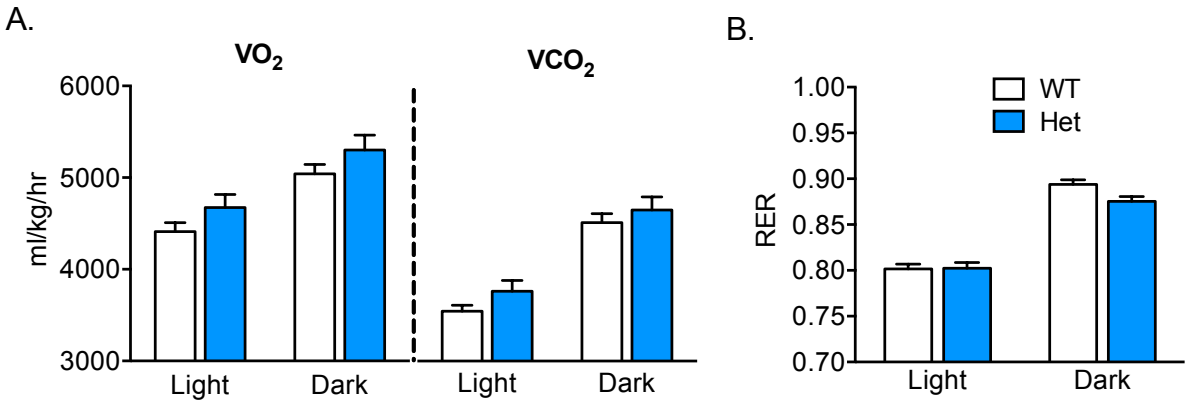

Supplemental Figure 6. CLAMS analysis does not reveal differences in metabolic parameters in p85$^{WT/R649W}$ mice. (A) oxygen consumption (VO_2) and carbon dioxide production (VCO_2) and **(B)** respiratory exchange ratio (RER) data were obtained from 10 week male study group mice (N=6). Results are shown as mean ± SEM.

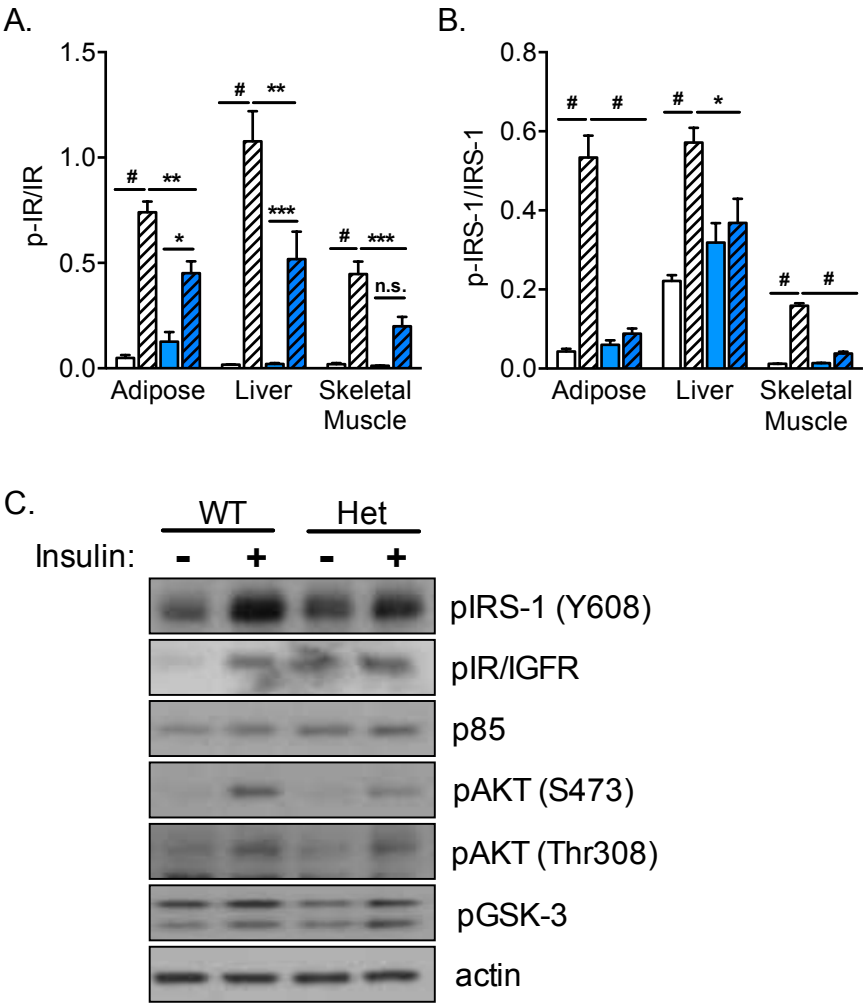

Supplemental Figure 7. Reduced insulin signaling in insulin-sensitive tissues of p85$^{WT/R649W}$ animals. Quantitative analysis of immunoblots performed on lysates from adipose tissue, liver and skeletal muscle using (**A**) p-IR and (**B**) p-IRS-1. Data were derived from the experiment outlined in Figure 5A (N=5-6). (**C**) Insulin signaling in differentiated preadipocytes from subcutaneous adipose tissue of control and p85α$^{WT/R649W}$ animals (N=3). Results are expressed as mean ± SEM. (*, $p<0.05$; **, $p<0.01$; ***, $p<0.001$; #, $p< 0.0005$).

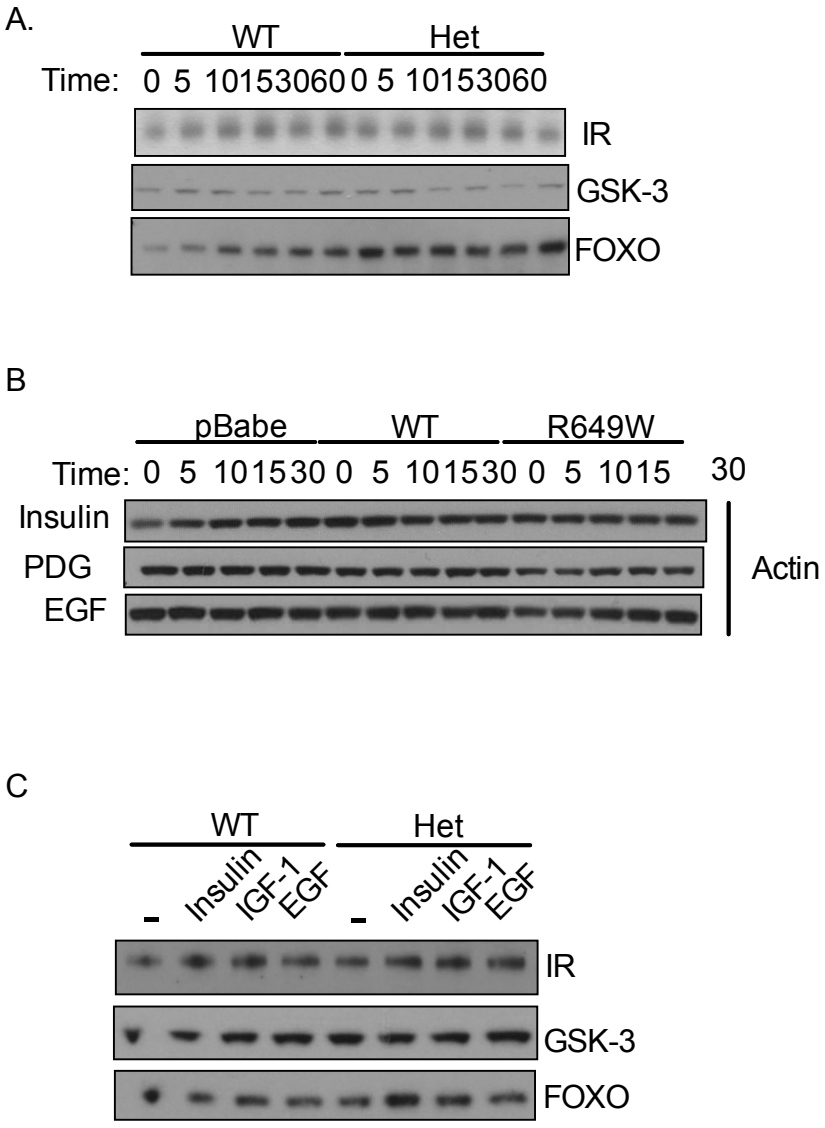

Supplemental Figure 8. Protein expression immunoblot controls. (A) Immunoblots of insulin receptor, GSK-3 and FOXO show protein expression is unchanged between WT and KI mutant mice in primary hepatocytes derived from WT and KI mutant mice Figure 5E. **(B)** Actin loading control for cells stimulated with Insulin and PDGF are equal to EGF in Figure 7A (actin for EGF stimulated cells is also shown in the original panel, Figure 7A. **(C)** Total levels of IR, GSK-3 and FOXO is comparable in primary hepatocytes derived from mice and stimulated with insulin, IGF-1 and EGF Figure 7C .

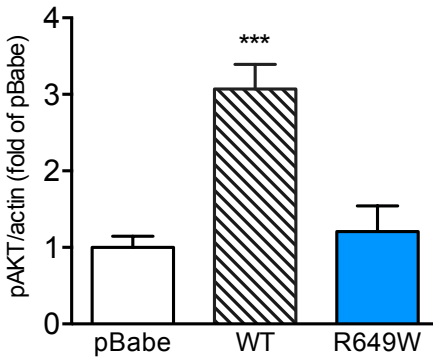

Supplemental Figure 9. Enforced expression of WT, but not the R649W mutant, restores the activation of AKT. Fold activation of AKT (S473) phosphorylation relative to the pBabe control (N=3). Results are expressed as mean ± SEM. (***, p<.001).

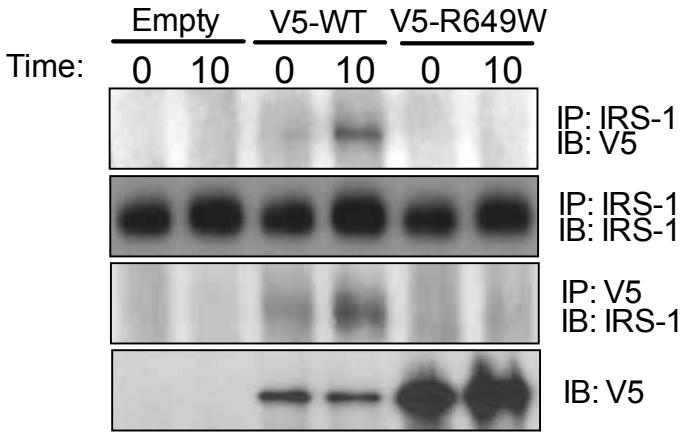

Supplemental Figure 10. The R649W mutant fails to interact with IRS-1. Co-immunoprecipitation of p85α and IRS-1 in 293T cells transiently transfected with expression plasmids encoding V5-tagged WT or R649W mutant p85α (N=2). Immunoprecipitation and immunoblotting was performed with the indicated antibodies.

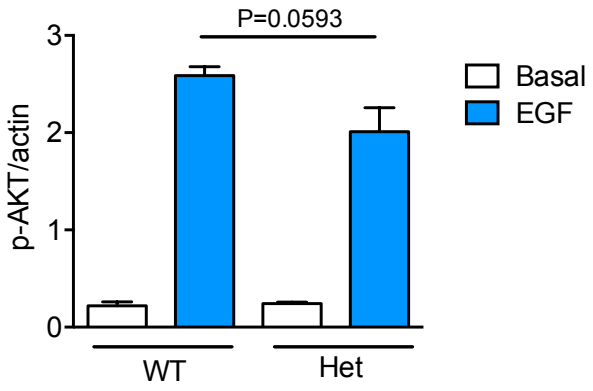

Supplemental Figure 11. The phosphorylation of AKT (S473) is moderately impaired in response to EGF. Quantification of immunoblots assessing the phosphorylation of AKT (S473)(N=5-7). Results are expressed as mean ± SEM.